A&A, 712, A146 (2026)
https://doi.org/10.1051/0004-6361/202659622
© The Authors 2026

Astronomy & Astrophysics

Formation of intermediate-mass black holes in young massive clusters detected with JWST: Analytic mass estimates

Viola Bocchi*, Matías Liempi, and Dominik R. G. Schleicher

Dipartimento di Fisica, Sapienza Università di Roma, Piazzale Aldo Moro 5, 00185 Rome, Italy

Received 26 February 2026 / Accepted 24 May 2026

ABSTRACT

The *James Webb* Space Telescope (JWST) has revealed a population of dense stellar systems at high redshifts, including the "Cosmic Gems" arc ($z \sim 10.2$) and the "Firefly Sparkle" ($z \sim 8.3$). With masses in the range $10^5\,M_\odot$–$10^7\,M_\odot$ and half-mass radii in the range ~0.4–15 pc, these systems are ideally suited to form intermediate-mass black holes (IMBHs) via collision-based models. Since direct N-body simulations are unfeasible for such a large population, and given the high masses in many of the clusters, we estimated the IMBH masses formed via runaway stellar collisions in these specific environments utilizing a Fokker-Planck model together with an analytical framework for runaway collisions and mass loss through winds, which has been validated against direct N-body simulations of compact star clusters. We applied this model to a sample of massive high-redshift clusters observed with JWST. Our estimates yield typical IMBH masses in the range $\sim 10^2\,M_\odot$ to $\sim 4 \times 10^3\,M_\odot$, implying typical formation efficiencies on the few percent level. The extreme compactness of the Cosmic Gems clusters ($R_h \sim 1$ pc) facilitates the formation of black hole seeds with high masses of 1600–2700 $M_\odot$. The low metallicity ($Z \lesssim 0.02\,Z_\odot$) is a critical factor for retaining the seed mass despite stellar winds. We further demonstrate that the efficiencies obtained here are consistent with expectations based on direct N-body simulations. Our results suggest that these dense, metal-poor clusters are viable factories for heavy seeds that are capable of growing into the supermassive black holes observed in the early Universe.

Key words. stars: kinematics and dynamics – stars: massive – galaxies: high-redshift – quasars: supermassive black holes – galaxies: star clusters: general

1. Introduction

The *James Webb* Space Telescope (JWST)[1] has provided abundant results pointing to very massive and dense systems at high redshifts, including systems with high star formation efficiencies. Some of the first galaxies detected initially were even considered to be more massive than they should be within the Λ cold dark matter framework (e.g., Labbé et al. 2023), a fact that was later attributed to the active galactic nucleus contamination of these sources (Chworowsky et al. 2024). While accounting for the active galactic nucleus component reduces the calculated stellar mass, the galaxies are still more abundant than previously expected, a result consistent with increased star formation efficiencies implying a shallower evolution of the volume density (Somerville et al. 2025).

A new class of high-redshift sources discovered by JWST are the little red dot (LRD) galaxies (Matthee et al. 2024; Greene et al. 2024; Akins et al. 2025; Zhang et al. 2025), which occur predominantly at redshifts of 4–8. They are highly compact objects with typical diameters of less than 300 pc and red, typically V-shaped spectra. Their luminosity has been interpreted as being due to stellar luminosities, which implies high central stellar densities with a median of $\sim 10^4\,M_\odot\,pc^{-3}$ and extending to maximum values of $\sim 10^8\,M_\odot\,pc^{-3}$ (Guia et al. 2024). Because of this, these systems were proposed to be ideal environments for the formation of supermassive black holes (SMBHs) via collision-based channels (Escala et al. 2025; Pacucci et al. 2025; Dekel et al. 2025).

The presence of high stellar densities is not restricted to LRDs or some special objects but is a more generic phenomenon in the early Universe. JWST has detected young massive clusters (YMCs) in several high-redshift galaxies via strong gravitational lensing. For example, Vanzella et al. (2022a) detected YMCs in the strongly lensed Sunburst Lyman-continuum galaxy at $z = 2.37$, with dynamical cluster masses of order $10^7\,M_\odot$. Vanzella et al. (2022b) found massive $10^6\,M_\odot$ clusters in the Hubble Frontier Field A2744 at redshift $z = 4$. Adamo et al. (2024) inferred bound massive clusters in the Cosmic Gems, an ultraviolet-faint galaxy at $z \sim 10.2$, with high stellar surface densities of $10^5\,M_\odot\,pc^{-2}$ (see also Messa et al. 2026; Vanzella et al. 2026). At redshift $z = 8.296$, Mowla (2024) found a set of massive clusters cocooned in a diffuse arc termed the Firefly Sparkle. The fact that several such systems were found, despite the requirements for strong gravitational lensing, suggests they were not uncommon in the early Universe. The high densities and masses in these systems suggest they are potentially relevant as formation sites of intermediate-mass black holes (IMBHs).

Particularly relevant black hole formation scenarios in this context are the collision-based scenarios (Devecchi & Volonteri 2009; Devecchi et al. 2012; Sakurai et al. 2017; Reinoso et al. 2018, 2020; Vergara et al. 2021; Liempi et al. 2025). Escala (2021) show using observational data that SMBHs are present in systems where the collision timescale is shorter than the age of the system, while systems with long collision times exhibit stable nuclear star clusters without SMBHs. A systematic influence of the collision timescale on the efficiency to form a central massive object was demonstrated by Vergara et al. (2023, 2024). The efficient formation of very massive objects in systems

*Corresponding author: bocchi.2109451@studenti.uniroma1.it
[1] JWST: https://science.nasa.gov/mission/webb/

Open Access article, published by EDP Sciences, under the terms of the Creative Commons Attribution License (https://creativecommons.org/licenses/by/4.0), which permits unrestricted use, distribution, and reproduction in any medium, provided the original work is properly cited.
This article is published in open access under the Subscribe to Open model. Subscribe to A&A to support open access publication.

with short collision timescales was recently demonstrated via direct N-body simulations by Vergara et al. (2023), Rantala et al. (2025), Rantala & Naab (2025), Vergara et al. (2025, 2026).

Several variants of such collision-based channels exist; for example, the presence of gas can further support the formation of massive objects through the interplay of collisions and accretion (Boekholt et al. 2018; Tagawa et al. 2020; Askar et al. 2022; Schleicher et al. 2022, 2023). Potentially important channels also include the contraction of black hole clusters in the centers of nuclear star clusters (Davies et al. 2011; Lupi et al. 2014; Kroupa et al. 2020; Chassonnery & Capuzzo-Dolcetta 2021; Gaete et al. 2024).

Of course, other black hole formation channels are also potentially conceivable. Intermediate-mass black holes could be remnants of the first massive stars (Bromm et al. 2002; Abel et al. 2002; Yoshida et al. 2008), or they could be the outcome of massive black hole formation via direct collapse (e.g., Koushiappas et al. 2004; Bromm & Loeb 2003; Wise et al. 2008; Begelman & Shlosman 2009; Schleicher et al. 2010; Latif et al. 2013). The relation between direct collapse and the collision-based models is not fully clear, and numerical simulations have shown that it is very difficult to bring all of the gas into a central massive object without fragmentation (e.g., Latif et al. 2015, 2016). On the other hand, gravitational torques can lead to the mergers of potential fragments with the central massive object even if fragmentation happens (Inayoshi & Haiman 2014; Latif & Schleicher 2015; Suazo et al. 2019), providing a possible intermediate regime in between a "pure" direct collapse and a star-cluster-based scenario. In that sense, direct collapse can be considered as a case of failed star cluster formation, where gravity was so efficient that a stable cluster was unable to form.

In this work we studied the massive dense clusters detected by JWST in high-redshift galaxies and aimed to determine their potential to form IMBHs. In particular, we aim to provide a conservative mass estimate by employing standard Fokker-Planck models for the dynamical evolution of the star clusters together with well-established results from stellar dynamics regarding the mergers of stars in dense environments (see Portegies Zwart & McMillan 2002). Our methodology is outlined in Sect. 2, and the main results are presented in Sect. 3. A summary and discussion is given in Sect. 4.

2. Methodology

In this section we first describe the details of the Fokker-Planck approach adopted here in Sect. 2.1. The initial conditions, and dynamical evolution of the systems are described in Sect. 2.2. The details of the black hole formation prescription are given in Sect. 2.3. Finally, in Sect. 2.4, we compare our results against N-body and Monte-Carlo models.

2.1. Fokker-Planck model

We used a high-accuracy finite-element method for the Fokker–Planck equation. The solver `PhaseFlow` is publicly available as part of the `Agama`[2] library (Vasiliev 2017, 2019).

Traditionally, the 1D orbit-averaged Fokker-Planck equation is expressed in terms of the energy E that in the flux-conservative form (e.g., Cohn 1980; Binney et al. 2009; Vasiliev 2017) is written as

$$\frac{\partial[f(E,t)g(E)]}{\partial t} = -\frac{\partial \mathcal{F}(E,t)}{\partial E}, \tag{1}$$

where $f(E,t)$ is the distribution function, $g(E)$ is the density of states defined as the partial derivative of the phase volume respect to the energy, and $\mathcal{F}(E,t)$ is the flux in energy space.

In `PhaseFlow`, the Fokker-Planck formalism is reformulated and uses the phase volume (h; defined as the volume of phase space enclosed by the energy hypersurface) as argument of the distribution function instead of the energy (E). Furthermore, it is possible to add a source term, s (e.g., to mimic star formation in clusters) and a sink term, νf (e.g., loss-cone draining rate), which results in the following expression:

$$\frac{\partial f(h,t)}{\partial t} = -\frac{\partial \mathcal{F}(h,t)}{\partial h} + s(h,t) - \nu(h,t) f(h,t), \tag{2}$$

with the distribution function $f(h,t)$ and the flux $\mathcal{F}(h,t)$ both now as a function of the phase volume. We here adopted $s(h,t) = 0$ and $\nu(h,t) = 0$, as we neglected star formation and assumed that an IMBH is not present, at least initially (and thus no loss cone effects). The flux through the phase volume is given as

$$-\mathcal{F}(h,t) = A(h) f(h,t) + D(h)\frac{\partial f(h,t)}{\partial h}, \tag{3}$$

with $A(h)$ and $D(h)$ the advection and diffusion coefficients, respectively.

In our model, we adopted a logarithmically spaced phase volume grid that contains 200 points. The minimum value ($h_{\rm min}$) was set to 10^{-20}, while the maximum value adopted was $h_{\rm max} = 10^3$, In our adopted virial units ($G = M = 1$), the total bound phase volume of the cluster is of order unity. Therefore, $h_{\rm max} = 10^3$ safely over-encompasses the bound phase space, ensuring accurate energy diffusion for loosely bound stars approaching the escape energy without boundary truncation. Conversely, because the core phase volume scales roughly as $h_{\rm core} \propto M_c^{3/2} r_c^{3/2}$, it drops exponentially during deep core collapse. The extreme lower bound of $h_{\rm min} = 10^{-20}$ is mathematically required to maintain flux conservation and continuously resolve the distribution function as the core radius (r_c) shrinks and the central density diverges. We used the Chang & Cooper (1970) discretization scheme with a timestep adaptively set with an accuracy parameter $\epsilon = 10^{-4}$ to ensure flux conservation.

2.2. Initial conditions and dynamical evolution of the system

The Fokker-Planck model implicitly assumes that all our clusters are composed of equal-mass stars spatially distributed following a Plummer density profile (Plummer 1911),

$$\rho(r) = \frac{3M}{4\pi b^3}\left(1 + \frac{r^2}{b^2}\right)^{-\frac{5}{2}}, \tag{4}$$

where M is the total mass of the system and b is the Plummer radius. For the simulations, we adopted virial units ($G = M = 1$) with a total energy of $E_{\rm tot} = -1/4$. This scaling constrains the Plummer scale radius to $b \approx 0.589$ (specifically $b = 3\pi/16$ in standard virial units). The properties of the high-redshift star clusters, which we employ here as initial conditions, are summarized in Table 1. Assuming equal-mass stars is clearly a simplified assumption, as realistic star clusters could instead evolve on the mass segregation timescale, which is shorter than

[2] https://github.com/GalacticDynamics-Oxford/Agama

the relaxation time. Considering mass segregation effects further would favor the subsequent formation of a central massive object. The Fokker-Planck model adopted here will therefore allow us to obtain a conservative estimate, while the evolution in real star clusters is potentially accelerated. The relaxation time of the system is given as

$$t_{\rm relax} = \frac{0.206 M^{1/2} b^{3/2}}{G^{1/2} m_\star \ln \Lambda}, \quad (5)$$

where $m_\star$ represents the individual stellar mass and $\ln \Lambda = \ln \gamma N$ is the Coulomb logarithm, where $\gamma = 0.4$ is adopted for systems composed by equal-mass stars (Spitzer 1987). In consequence the number of stars N is given by $N = M_{\rm cl}/1\,{\rm M}_\odot$ (i.e., assuming solar-mass stars) with $M_{\rm cl}$ the stellar mass of the cluster in solar masses.

As the YMCs observed with JWST have typical ages of a few tens of millions of years (Vanzella et al. 2022a,b, 2023; Adamo et al. 2024; Mowla 2024), we here evolved the Fokker-Planck model for a characteristic timescale of about 100 Myr, to account for the fact that the evolution in realistic star clusters will be faster due to mass segregation effects compared to models assuming equal mass stars. Indeed, equal-mass systems typically reaches core collapse on a timescale of $\sim 15 t_{\rm relax}$ (Cohn 1980), while the presence of a stellar mass function can shorten this process to as little as $2-3\,t_{\rm relax}$ (e.g., Gürkan et al. 2004) as massive stars rapidly sink to the center. In real systems, there is even the possibility of preexisting central cores resulting from the process of star cluster formation, while our model conservatively starts from a Plummer sphere for the initial distribution of stars.

2.3. Black hole mass estimation

The contraction of the star cluster as described through the Fokker-Planck model will lead to the formation of a central core within the star cluster. The growth of central massive objects in such environments via runaway collisions has been studied by Portegies Zwart & McMillan (2002), Katz et al. (2015), Rantala & Naab (2025), Vergara et al. (2025, 2026), where a detailed analytical framework has been provided by Portegies Zwart & McMillan (2002) considering the migration times of stars of different masses. This model has been recently extended by Fujii et al. (2024), Pacucci et al. (2025) to account for the mass loss through winds by the very massive star (VMS). The maximum mass (assuming that all the collisions involve the same star) is given by

$$\dot{M}_{\rm acc} = \dot{N}_{\rm coll} \langle \delta m \rangle_{\rm coll}, \quad (6)$$

with $\dot{N}_{\rm coll}$ the average collision rate and $\langle m \rangle_{\rm coll}$ the average mass increase per collision.

The Portegies Zwart & McMillan (2002) suite of simulations showed that collisions between stars generally occur in dynamically formed ("three-body") binaries and, in consequence, the average collision rate ($\dot{N}_{\rm coll}$) is related to the binary formation rate. Neglecting stellar evolution effects and assuming the large-scale energy flux in the cluster to be powered by binary heating in the core, the average collision rate is well approximated by

$$\dot{N}_{\rm coll} \approx 10^{-3} f_c \frac{N}{t_{\rm relax}}, \quad (7)$$

where $f_c \leq 1$ represents the effective fraction of dynamically formed binaries that produce a collision, $t_{\rm relax}$ is the relaxation time, and N the number of stars in the system, estimated as $M_{\rm cl}/1\,{\rm M}_\odot$. We here employed the value of $f_c = 0.8$ as found empirically by Fujii et al. (2024) and later adopted in the work of Pacucci et al. (2025). While the negligence of stellar evolution effects is clearly a simplifying assumption, in the following we verify the results obtained with this model through the

Table 1. Properties of the high-redshift massive star clusters.

Cluster ID	$M_{\rm cl}$ [$M_\odot$]	R_h [pc]	Z [$Z_\odot$]
A1[a]	2.45×10^6	1.1	0.005
B1[a]	2.65×10^6	1.1	0.005
C1[a]	1.13×10^6	<1	0.005
D1[a]	1.13×10^6	0.6	0.005
E1[a]	1.01×10^6	0.4	0.005
FF-1[b]	1.82×10^5	<6.8	0.02
FF-2[b]	2.29×10^6	<6.2	0.02
FF-3[b]	4.57×10^5	<5.1	0.02
FF-4[b]	1.38×10^5	<4.9	0.02
FF-5[b]	2.57×10^5	<4.6	0.02
FF-6[b]	2.04×10^5	<4.3	0.02
FF-7[b]	1.42×10^5	<4.1	0.02
FF-8[b]	1.02×10^5	<3.9	0.02
FF-9[b]	9.33×10^4	<4.2	0.02
FF-10[b]	1.00×10^6	<4.3	0.02
5.1a[c]	9.10×10^6	8.1	0.02
5.1b[c]	1.02×10^7	8.2	0.02
5.1c[c]	1.13×10^7	9.6	0.02
5.1h[c]	1.22×10^7	10.8	0.02
5.1i[c]	5.10×10^6	7.8	0.02
5.11[c]	1.17×10^7	8.5	0.02
5.1m[c]	1.28×10^7	<19.5	0.02
5.1n[c]	1.71×10^7	<20.4	0.02
5.2h[c]	5.40×10^6	4.8	0.02
5.3h[c]	1.47×10^7	23.7	0.02
5.4a[c]	3.20×10^6	5.4	0.02
5.5a[c]	3.00×10^6	7.9	0.02
5.6a[c]	3.20×10^6	9.0	0.02
5.8d[c]	7.10×10^6	20.2	0.02
5.9d[c]	4.50×10^6	21.4	0.02
5.11d[c]	2.40×10^6	15.0	0.02
5.16d[c]	5.50×10^6	22.0	0.02
5.12g[c]	1.00×10^6	2.9	0.02
5.13g[c]	1.00×10^5	0.9	0.02
5.15h[c]	1.00×10^5	1.3	0.02
3.1a[d]	4.10×10^6	13.8	0.02
3.2a[d]	7.00×10^5	3.2	0.02
3.3a[d]	9.00×10^5	11.4	0.02
3.1b[d]	3.60×10^6	15.3	0.02
3.2b[d]	5.00×10^5	3.0	0.02
3.3b[d]	1.20×10^6	10.9	0.02
3c[d]	1.65×10^8	279.4	0.02
1b[e]	7.10×10^6	1.4	0.02
2b[e]	3.90×10^6	6.3	0.02
3b[e]	1.10×10^6	6.1	0.02
4b[e]	1.01×10^7	24.8	0.02
5b[e]	3.10×10^6	4.9	0.02
6b[e]	3.30×10^6	8.5	0.02

Notes. [(a)] Adamo et al. (2024) [(b)] Mowla (2024) [(c)] Vanzella et al. (2022a) [(d)] Vanzella et al. (2022b) [(e)] Vanzella et al. (2023).

comparison with direct N-body simulations that include stellar evolution to show that the simplification still leads to reasonable results.

The average mass increase per collision is given by

$$\langle \delta m \rangle_{\rm coll} \simeq 4 \frac{t_{\rm relax}}{t} \langle m \rangle \ln \Lambda, \tag{8}$$

where $\langle m \rangle = 1\,{\rm M}_\odot$, and again $\ln \Lambda = \ln 0.4N$. Thus, replacing Eqs. (7) and (8) in Eq. (6), the mass growth of the VMS due to stellar collisions is

$$\dot{M}_{\rm acc} = 4 \times 10^{-3} f_c \ln \Lambda \frac{M_{\rm cl}}{t}. \tag{9}$$

Following the procedure of Fujii et al. (2024), Eq. (9) can be rewritten defining a "supply rate" $\dot{M}_{\rm cl} = M_{\rm cl}/t$. However, we had to account for the fact that the runaway collision process is dynamically restricted to the dense central region of the cluster. While the global energy budget is determined by the total cluster mass, the immediate mass reservoir available for the growth of the VMS is the cluster core. Direct N-body simulations, for example by Arca Sedda et al. (2023), Vergara et al. (2025), Rantala et al. (2026), show that the timescale over which stars are supplied to the central object is comparable to the relaxation timescale of the central core, so we estimated t by evaluating the relaxation time (Eq. (5)) and using the core mass ($M_{\rm core}$), which we also employed to estimate the stellar mass reservoir. We identified the core radius ($r_{\rm core}$) as the point where the density profile drops to half its central value and defined $M_{\rm core}$ as the enclosed mass at this radius. The effective supply rate feeding the VMS is therefore defined as SF $= M_{\rm core}/t_{\rm relax,core}$, where $t_{\rm relax,core}$ is the relaxation time of the core.

Substituting $M_{\rm cl}$ with $M_{\rm core}$ in Eq. (9), the "accretion" rate becomes dependent on the Coulomb logarithm $\ln \Lambda$. For the massive clusters considered in this work ($N \sim 10^5$–10^6), the Coulomb logarithm is in the range $\ln \Lambda \approx 10$–12. Thus, the pre-factor $0.003 \ln \Lambda$ is well approximated by a constant efficiency of ≈0.03. This yields the final expression used in our model:

$$\dot{M}_{\rm acc} \approx 0.03 \times \frac{M_{\rm core}}{t_{\rm relax,core}}. \tag{10}$$

This "supply" rate is then balanced against the wind mass loss rate. The mass loss rate (assuming fixed metallicity) is given by Vink (2018)

$$\log_{10}\left(\frac{\dot{M}_{\rm wind}}{{\rm M}_\odot\,{\rm yr}^{-1}}\right) = -9.13 + 2.1 \log_{10}\left(\frac{M_{\rm VMS}}{{\rm M}_\odot}\right) + 0.74 \log_{10}\left(\frac{Z}{Z_\odot}\right). \tag{11}$$

The time evolution of the mass of the VMS is given by the balance between mass gain via collisions and mass loss due to stellar winds:

$$\dot{M}_{\rm VMS} = \dot{M}_{\rm acc} - \dot{M}_{\rm wind}. \tag{12}$$

We assumed here that the VMS grows until the mass loss from the wind becomes comparable to the mass growth via collisions. Some uncertainty in this approach lies in the timescale that is adopted here for the timescale entering in Eq. (9), which could vary for example in the presence of rotation or depending on the binary fraction. However, given the balance in Eq. (12) between mass gain by accretion and mass loss by wind, the dependence of the final mass of the VMS on the timescale is relatively weak and would scale as $t^{1/2.1} \sim t^{0.48}$. A change in the timescale by a factor of 10 thus will not affect the result by more than a factor of 3, consistent with the level of uncertainty in the absence of detailed N-body simulations.

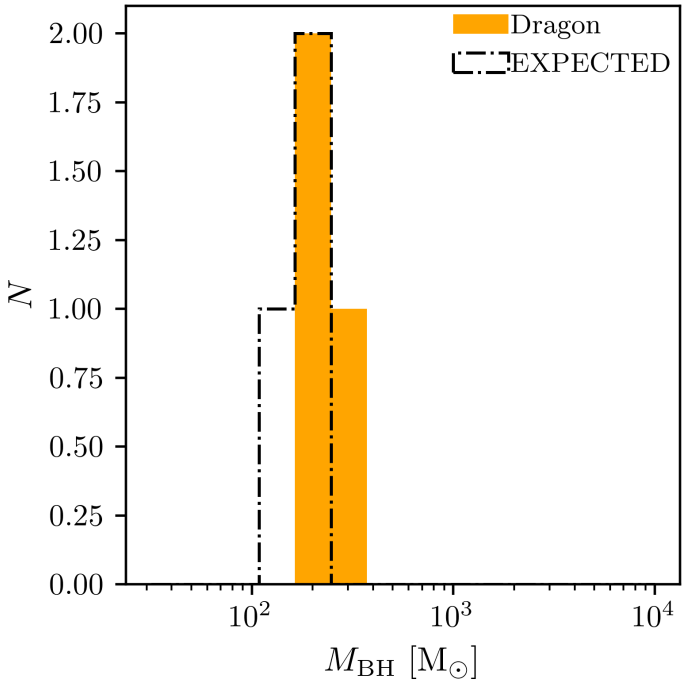


Fig. 1. Comparison of the black hole mass distribution. The dashed black line shows the prediction from the framework presented here, and the orange histogram represents the results from the Dragon simulations (Arca Sedda et al. 2023).

To estimate the final black hole seed mass ($M_{\rm BH}$), we assumed that the VMS collapses directly into a black hole at the end of its life. Given the high masses ($>10^3\,{\rm M}_\odot$) and low metallicities considered in this work, we assumed negligible mass loss during the collapse phase, setting $M_{\rm BH} \approx M_{\rm VMS}$.

2.4. Comparison with numerical simulations

Many of the star clusters found by JWST are quite massive, making direct N-body simulations very difficult or essentially unfeasible. We thus necessarily needed to employ a simplified framework in order to derive estimates for the masses of possible IMBHs. Nonetheless, it is instructive to test our model framework in the regime where such a comparison is possible. For this purpose, we utilized the large N-body simulations from Arca Sedda et al. (2023), Vergara et al. (2025), which are based on the NBODY6++GPU and MOCCA codes, as well as the FROST clusters presented by and Rantala et al. (2026). Both approaches incorporate up-to-date stellar evolution routines (SSE/BSE) alongside specific prescriptions for the formation and dynamical evolution of VMSs.

To ensure a consistent comparison, we initialized our semi-analytic model using the cluster parameters provided in the original papers. In Fig. 1 we compare our results to the DRAGON II simulations (Arca Sedda et al. 2023), which predict IMBH masses of ∼150–350 $M_\odot$. These are slightly underestimated in our model framework, which predicts typical values of 100–250 $M_\odot$. Figure 2 illustrates the results of this cross-check with the Vergara et al. (2025) simulations. The blue histogram shows the distribution of black hole masses obtained from the Vergara et al. (2026) simulations, while the dot-dashed

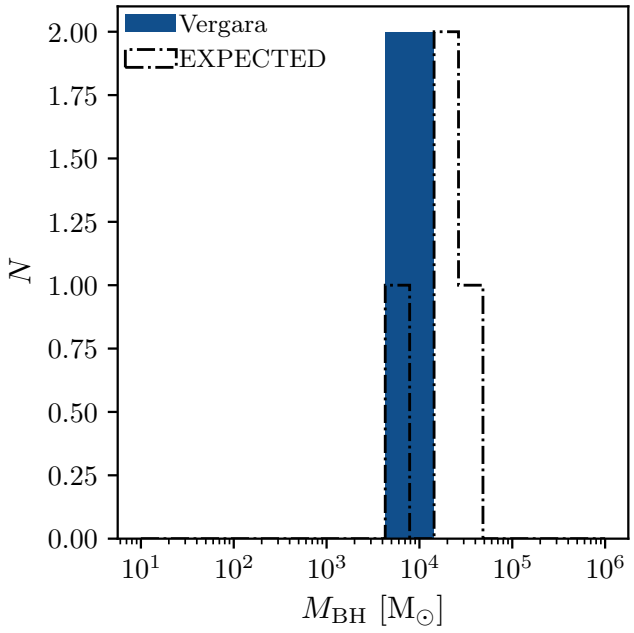


Fig. 2. Comparison of the black hole mass distribution. The dashed black line shows the prediction from the framework presented here, and the blue histogram represents the results from the N-body simulations of Vergara et al. (2025).

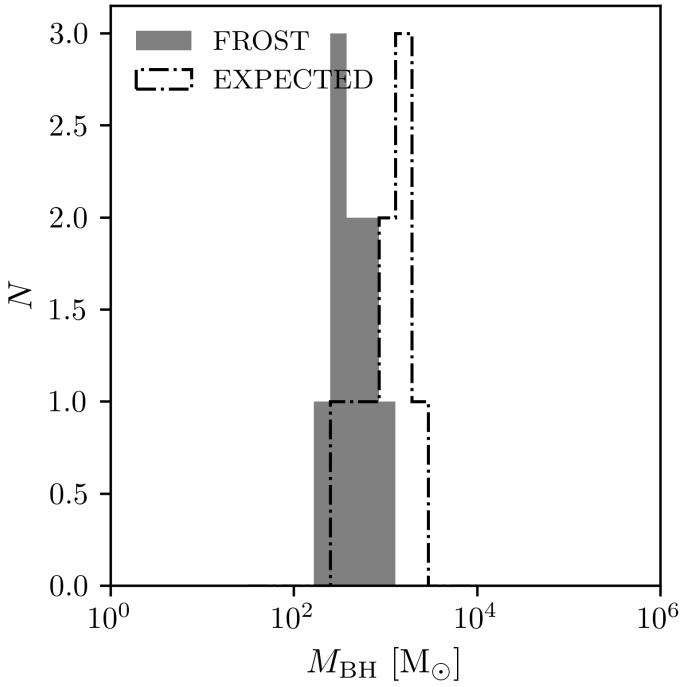


Fig. 3. Comparison of the black hole mass distribution. The dashed black line shows the prediction from the framework presented here, and the gray histogram represents the results from the FROST simulations (Rantala et al. 2026).

black step line shows the mass distribution predicted by our analytic model for the same set of clusters. Our model framework predicts masses of 8×10^3–$5 \times 10^4\,M_\odot$ for the Vergara et al. (2026) simulations, while the simulations themselves derived masses in the range 4×10^3–$1.5\times10^4\,M_\odot$. In this case, the model captures the magnitude of the expected masses but with deviations including a factor of 3–5.

In Fig. 3 we compare with the FROST clusters by Rantala et al. (2026), where the original simulations predicted masses of ∼200–1000 $M_\odot$, while our framework suggests masses of 300–3000 $M_\odot$. In this case our framework shows an uncertainty within a factor of 2–3. In summary, we can say that our model framework provides the order-of-magnitude of the massive objects formed in these simulations, with expected deviations of around half an order of magnitude when compared to detailed N-body simulations. While our model does not include an explicit treatment of the mass loss during collisions, we note that such a treatment is included in the simulations of Vergara et al. (2025), Rantala et al. (2026) following Glebbeek & Pols (2008), Glebbeek et al. (2009, 2013) and thus consistent with the overall uncertainty considered here.

3. Results

In the following subsections, we employ the framework presented above to the different systems for which JWST has provided measurements of the masses and radii of YMCs. We also aim to summarize global scaling relations and efficiencies.

3.1. Fokker-Planck results

The results from the Fokker-Planck model indicate the evolution of the star clusters we can expect after a timescale of 100 Myr, assuming clusters of equal mass stars. In real stellar clusters, as discussed above, the evolution can be easily accelerated at least by a factor of a few, considering that the mass segregation timescale is shorter than the relaxation time as well as even the presence of a possible primordial mass segregation. The expected properties of the resulting cores are given in Fig. 4 showing core mass ($M_{\rm core}$) as a function of core radius ($r_{\rm core}$). The core masses tend to be in the range from $10^4\,M_\odot$ up to $10^6\,M_\odot$, with radii in the range from ∼0.4 pc up to ∼15 pc. We note that the cores from the Adamo et al. (2024) sample are particularly compact, on the order of ∼0.5 pc, and that the Vanzella et al. (2023) sample includes some clusters with core radii of ∼0.6–0.8 pc, even if most of their cores have radii of ∼1.5–15 pc. The data from Messa et al. (2026), Mowla (2024) share the mass range but tend to be at the larger radii. The trends of the cores follow the underlying properties of the star clusters. Globally, this is consistent both with expectations from numerical simulations, which show that about 10% of the star clusters might be on the rather compact side (Grudić et al. 2023), and with the properties of star clusters in the local Universe, where again about 10% show rather compact radii compatible with the JWST clusters (Brown & Gnedin 2021). The latter is also compatible with the Marks & Kroupa (2012) relation, indicating compact cluster radii at the initial formation time of the clusters.

3.2. Compact clusters in the Cosmic Gems Arc

We next used the framework laid out in Sect. 2.3 to estimate the masses of IMBHs that could form in the dense JWST clusters in a collision-based scenario. We emphasize that these estimates are subject to uncertainties of at least a factor of a few, as most of the clusters are in a regime where direct N-body simulations are not feasible. Nonetheless deriving such estimates based on the previous results of Portegies Zwart & McMillan (2002) and

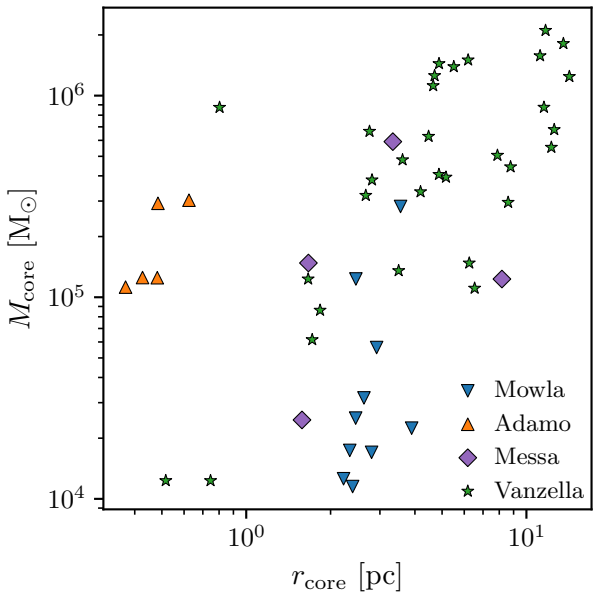


Fig. 4. Mass of the core as a function of the core radius. Blue triangles are clusters from Mowla (2024), orange triangles clusters from Adamo et al. (2024), purple diamonds data from Messa et al. (2026), and green stars data from Vanzella et al. (2022a,b, 2023).

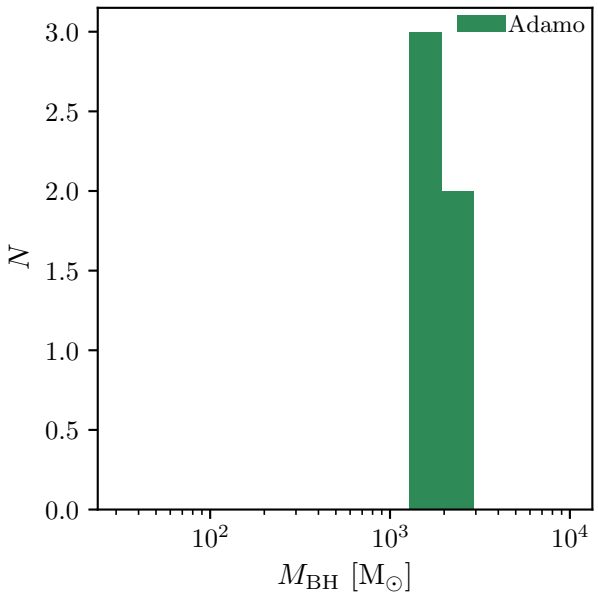


Fig. 5. Mass distribution of estimated black hole masses in the data sample of Adamo et al. (2024).

Table 2. Estimated core and black hole properties for the Cosmic Gems cluster sample.

ID	$M_{\rm cl}$ [$M_\odot$]	R_h [pc]	$M_{\rm core}$ [$M_\odot$]	$R_{\rm core}$ [pc]	$M_{\rm BH}$ [$M_\odot$]
A1	2.45×10^6	1.10	3.03×10^5	0.62	2.68×10^3
B1	2.65×10^6	0.90	2.92×10^5	0.48	2.64×10^3
C1	1.13×10^6	0.90	1.25×10^5	0.48	1.76×10^3
D1	1.13×10^6	0.80	1.25×10^5	0.43	1.76×10^3
E1	1.01×10^6	0.70	1.12×10^5	0.37	1.67×10^3

Notes. Properties are derived from the cluster data presented in Adamo et al. (2024).

Table 3. Estimated core and black hole properties for the Firefly Sparkle cluster sample.

ID	$M_{\rm cl}$ [$M_\odot$]	R_h [pc]	$M_{\rm core}$ [$M_\odot$]	$R_{\rm core}$ [pc]	$M_{\rm BH}$ [$M_\odot$]
FF-1	1.82×10^5	6.80	2.24×10^4	3.89	2.42×10^2
FF-2	2.29×10^6	6.20	2.82×10^5	3.55	8.07×10^2
FF-3	4.57×10^5	5.10	5.63×10^4	2.92	3.74×10^2
FF-4	1.38×10^5	4.90	1.70×10^4	2.80	2.12×10^2
FF-5	2.57×10^5	4.60	3.17×10^4	2.63	2.85×10^2
FF-6	2.04×10^5	4.30	2.52×10^4	2.46	2.55×10^2
FF-7	1.41×10^5	4.10	1.74×10^4	2.34	2.14×10^2
FF-8	1.02×10^5	3.90	1.26×10^4	2.23	1.83×10^2
FF-9	9.33×10^4	4.20	1.15×10^4	2.40	1.76×10^2
FF-10	1.00×10^6	4.30	1.23×10^5	2.46	5.44×10^2

Notes. Properties are derived from the cluster data presented in Mowla (2024).

the framework of Pacucci et al. (2025) will be useful to assess the possible mass range of IMBHs that could be present.

The results for the clusters identified in the Cosmic Gems arc are presented in Table 2. These systems are characterized by their extreme compactness, with half-mass radii consistently around $R_h \approx 1$ pc despite having stellar masses of around $\sim10^6\,M_\odot$. The high stellar density facilitates a rapid core collapse, leading to substantial core masses ($M_{\rm core} \sim 1{-}3{\times}10^5\,M_\odot$). Consequently, our model predicts the formation of IMBHs with masses ranging from $\sim1.7{\times}10^3$ to $\sim2.7{\times}10^3\,M_\odot$. The low metallicity assumed for this high-redshift galaxy ($Z \approx 0.005\,Z_\odot$) further aids in retaining the accreted mass by reducing the efficiency of stellar wind mass loss during the VMS phase.

The results of the calculation are provided in Fig. 5. As the star clusters and cores have rather similar properties, the expected mass distribution of the IMBHs shows a clear peak around $\sim10^3\,M_\odot$, providing a significant potential to form quite massive black holes.

3.3. Extended clusters in the Firefly Sparkle

Table 3 summarizes the properties of the clusters associated with the Firefly Sparkle (Mowla 2024). In contrast to the Cosmic Gems, these clusters exhibit significantly larger radii ($R_h \sim 4{-}6$ pc) for typically lower total masses ($10^5{-}10^6\,M_\odot$). This lower dynamical density results in less massive cores ($M_{\rm core} \sim 10^4{-}3\times10^5\,M_\odot$; see Fig. 4), limiting the reservoir available for the runaway collision process. As a result, the predicted black hole masses are also reduced, with the distribution (Fig. 6) in the range $1.8\times10^2{-}8.1\times10^2\,M_\odot$. Within the sources investigated here, these objects are forming the lower boundary of expected IMBH masses.

3.4. Variable density candidates

The results for the cluster candidates identified by Messa et al. (2026) are listed in Table 4. This sample presents a diverse set of environments, ranging from compact ($R_h \sim 2.7$ pc) to extended

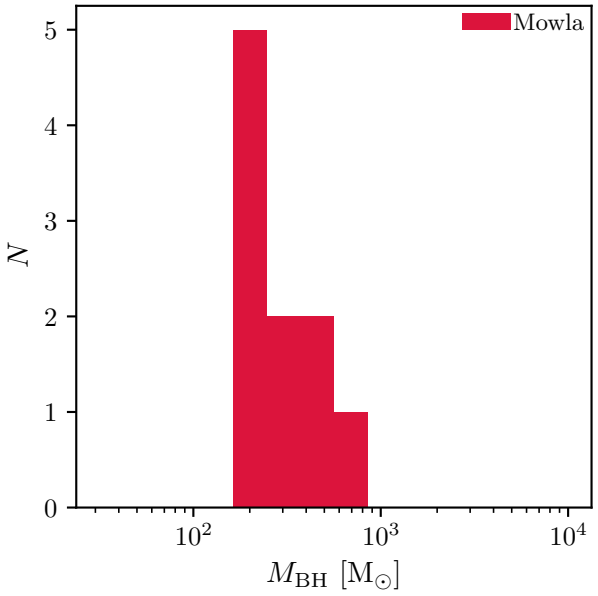


Fig. 6. Mass distribution of estimated black hole masses for the Mowla (2024) sample.

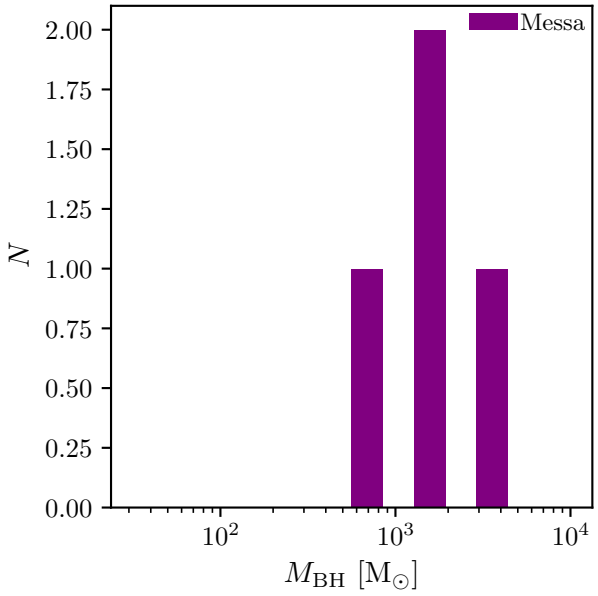


Fig. 7. Distribution of estimated black hole masses for the Messa et al. (2026) clusters.

Table 4. Core and black hole properties for the variable density candidates.

ID	$M_{\rm cl}$ [$M_\odot$]	R_h [pc]	$M_{\rm core}$ [$M_\odot$]	$R_{\rm core}$ [pc]	$M_{\rm BH}$ [$M_\odot$]
M1	4.80×10^6	5.82	5.91×10^5	3.34	3.69×10^3
M2	1.00×10^6	14.25	1.23×10^5	8.18	1.75×10^3
M3	2.00×10^5	2.76	2.46×10^4	1.58	8.13×10^2
M4	1.20×10^6	2.91	1.48×10^5	1.67	1.91×10^3

Notes. Properties are derived from the cluster data presented in Messa et al. (2026).

($R_h \sim 14$ pc) systems. Notably, the most massive cluster in this set (M1, $M_{\rm cl} \approx 4.8\times10^6\,M_\odot$) yields a black hole mass of $\sim3.7\times10^3\,M_\odot$. Despite the high total cluster mass, the black hole formation efficiency is moderated by the higher assumed metallicity ($Z = 0.1\,Z_\odot$), implying more mass loss through winds, and the larger radii compared to the Adamo et al. (2024) sample. The expected distribution of the IMBH masses is given in Fig. 7, with masses ranging from $\sim8.1\times10^2\,M_\odot$ to $\sim3.7\times10^3\,M_\odot$.

3.5. Massive young clusters in the Sunburst Arc and Frontier Fields

We next considered the results for the massive young clusters in the Sunburst Arc and other fields covered by Vanzella et al. (2022a,b, 2023). A summary of these clusters is provided in Table 5. These systems represent the high-mass end of our sample, with several clusters exceeding $10^7\,M_\odot$. While they are spatially extended (half-mass radii often >10 pc), the sheer magnitude of their stellar mass still leads to the production of very massive cores ($M_{\rm core} > 10^6\,M_\odot$), thereby compensating for the more extended radii. The expected distribution of IMBH masses is given in Fig. 8, showing a range of masses from $\sim1.8\times10^2\,M_\odot$ up to $\sim2.1\times10^3\,M_\odot$.

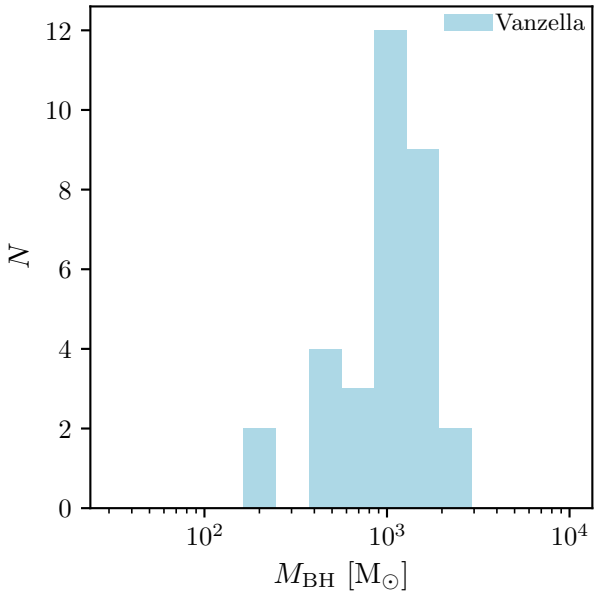


Fig. 8. Mass distribution of estimated black hole masses for the Vanzella et al. (2022a,b, 2023) samples.

3.6. Scaling relations and efficiency

To assess the results more globally, we show the estimated IMBH mass as a function of the core mass for the different samples in Fig. 9. We in general find that most of the dependence of the masses of the IMBHs is due to the mass budget available to go into collisions. A relevant additional factor is also the metallicity. As so far no individual metallicities are provided for each cluster (and their metallicities may be similar as long as they are in the same environment), we find a good relation between expected black hole mass versus star cluster mass within each given sample, due to the assumption of constant metallicity. On the other hand, the difference in metallicity between the different samples (particularly the relatively high-metallicity case in Mowla 2024) produces offsets between the

Table 5. Estimated core and black hole properties for the Sunburst Arc and Frontier Fields cluster samples.

ID	$M_{\rm cl}$ [$M_\odot$]	R_h [pc]	$M_{\rm core}$ [$M_\odot$]	$R_{\rm core}$ [pc]	$M_{\rm BH}$ [$M_\odot$]
5.1a	9.10×10^6	8.10	1.12×10^6	4.65	1.56×10^3
5.1b	1.02×10^7	8.20	1.26×10^6	4.70	1.64×10^3
5.1c	1.13×10^7	9.60	1.39×10^6	5.51	1.72×10^3
5.1h	1.22×10^7	10.80	1.50×10^6	6.19	1.79×10^3
5.1i	5.10×10^6	7.80	6.28×10^5	4.48	1.18×10^3
5.1l	1.17×10^7	8.50	1.44×10^6	4.88	1.75×10^3
5.1m	1.28×10^7	19.50	1.58×10^6	11.19	1.83×10^3
5.1n	1.71×10^7	20.40	2.11×10^6	11.70	2.10×10^3
5.2h	5.40×10^6	4.80	6.65×10^5	2.75	1.21×10^3
5.3h	1.47×10^7	23.70	1.81×10^6	13.55	1.96×10^3
5.4a	3.20×10^6	5.40	3.20×10^5	2.67	8.57×10^2
5.5a	3.00×10^6	7.90	3.33×10^5	4.19	8.73×10^2
5.6a	3.20×10^6	9.00	3.94×10^5	5.16	9.46×10^2
5.8d	7.10×10^6	20.20	8.75×10^5	11.55	1.38×10^3
5.9d	4.50×10^6	21.40	5.54×10^5	12.27	1.11×10^3
5.11d	2.40×10^6	15.00	2.95×10^5	8.61	8.25×10^2
5.16d	5.50×10^6	22.00	6.78×10^5	12.57	1.23×10^3
5.12g	1.00×10^6	2.90	1.23×10^5	1.66	5.44×10^2
5.13g	1.00×10^5	0.90	1.23×10^4	0.52	1.82×10^2
5.15h	1.00×10^5	1.30	1.23×10^4	0.75	1.82×10^2
3.1a	4.10×10^6	13.80	5.06×10^5	7.88	1.07×10^3
3.2a	7.00×10^5	3.20	8.62×10^4	1.83	4.59×10^2
3.3a	9.00×10^5	11.40	1.11×10^5	6.53	5.17×10^2
3.1b	3.60×10^6	15.30	4.43×10^5	8.78	1.00×10^3
3.2b	5.00×10^5	3.00	6.16×10^4	1.72	3.91×10^2
3.3b	1.20×10^6	10.90	1.48×10^5	6.25	5.93×10^2
3c	7.10×10^6	1.40	8.74×10^5	0.80	1.38×10^3
1b	3.90×10^6	6.30	4.80×10^5	3.61	1.04×10^3
2b	1.10×10^6	6.10	1.35×10^5	3.50	5.69×10^2
3b	1.01×10^7	24.80	1.24×10^6	14.23	1.63×10^3
4b	3.10×10^6	4.90	3.82×10^5	2.81	9.32×10^2
5b	3.30×10^6	8.50	4.06×10^5	4.87	9.60×10^2

Notes. Properties are derived from the cluster data presented in Vanzella et al. (2022a,b, 2023).

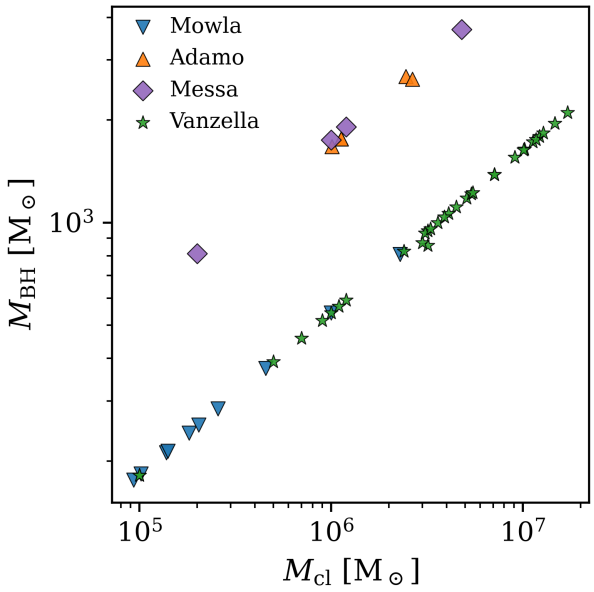


Fig. 9. Estimated IMBH mass ($M_{\rm BH}$) as a function of the stellar mass of the host cluster ($M_{\rm cl}$) for the different samples.

different relations. The differences in the radii do lead to fluctuations in these relations but they are not very strong. We do note in this respect that the largest variations in the core radii correspond to a factor of 2–3, and the mass accretion rate in Eq. (10) (Portegies Zwart & McMillan 2002) depends on the core mass, but not the core radius. We emphasize, nonetheless, that part of the absence of scatter is also due to the simplifying assumptions in our model; more scatter could be expected in direct N-body simulations or if different cluster properties are assumed or taken into consideration, for example in relation to primordial binaries or the rotation of the clusters.

For comparison with the work of Vergara et al. (2023, 2024), we quantified the expected formation efficiency of the IMBHs, which we defined as the expected mass of the IMBH divided by the total mass of the cluster. We normalized the cluster mass by the critical mass for runaway collisions, $M_{\rm crit}$, defined as $M_{\rm crit}(R_h) = R_h^{\frac{7}{3}}\left(\frac{4\pi m_\star}{3\Sigma_0 t_{\rm H} G^{\frac{1}{2}}}\right)^{\frac{2}{3}}$ (Vergara et al. 2023), where R_h is the radius of the system, $m_\star$ the mass of a single star, $t_{\rm H}$ the age of the system, and Σ_0 the effective cross section expressed as $\Sigma_0 = 16\sqrt{\pi}(1+\Theta)\,{\rm R}_\odot^2$, with $\Theta = 9.54\,[(m_\star\,{\rm R}_\odot)/(r_\star\,{\rm M}_\odot)]\left(100\,{\rm km\,s^{-1}}/\sigma\right)^2$ the Safronov number, where $R_\star$ is the radius of a single star (assumed to be sun-like), and $\sigma = \sqrt{GM_{\rm cl}/R_{\rm h}}$, which is the velocity dispersion under the assumption of virial equilibrium. The age of the systems is set to $t_{\rm H} = 100$ Myr for all the clusters as a conservative estimate assuming it as the characteristic timescale over which dynamical interactions can operate efficiently as previously discussed in Sect. 2.1.

Figure 10 presents the black hole formation efficiency ($\epsilon_{\rm BH} = [1 + M_{\rm BH}/M_{\rm cl}]^{-1}$) as a function of the critical mass ratio. The inset highlights the impact of metallicity. The clusters from Messa et al. (2026, purple diamonds), which were modeled with higher metallicity ($Z = 0.1\,{\rm Z}_\odot$), tend to show lower formation efficiencies compared to similarly massive but metal-poor systems. This suppression is a direct consequence of the metallicity-dependent wind mass loss (Eq. (11)), which erodes the VMS mass more effectively in chemically enriched environments. For comparison, we also provide the fit from Vergara et al. (2026) to the numerical simulation data that have explored the dependence of the efficiency parameter $\epsilon_{\rm BH}$ on the ratio $M/M_{\rm crit}$, given as

$$\epsilon_{\rm BH} = \left[1 + \exp\left(-4.63\left[\log\left(\frac{M}{M_{\rm crit}}\right) - 4\right]\right)\right]^{-0.1}. \quad (13)$$

We note that the fit aligns well with the data points including the expected scatter (e.g., Vergara et al. 2024), suggesting formation efficiencies in the few percent range. This is very reasonable as a result; in fact it seems very likely that clusters with larger formation efficiencies would be much more short-lived and thus very difficult to find via observations.

4. Summary and discussion

We estimated the masses of IMBHs formed in the massive young stellar clusters detected by JWST at high redshift using gravitational lensing techniques (Adamo et al. 2024; Vanzella et al. 2022a,b, 2023; Mowla 2024; Messa et al. 2026). As these clusters have large masses up to $10^7\,{\rm M}_\odot$, modeling via direct N-body

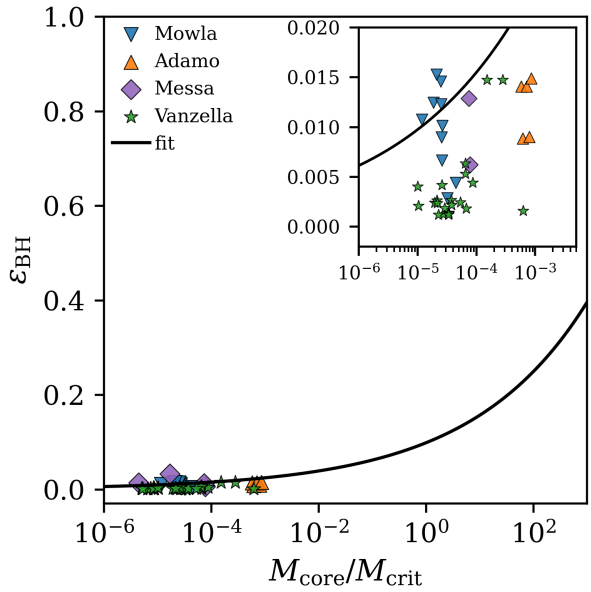


Fig. 10. Expected black hole formation efficiency as a function of $M/M_{\rm crit}$ from the model presented here compared to the fit from Vergara et al. (2026) described in Eq. (13).

simulations is impossible, and instead we employed an approximate methodology using Fokker-Planck models to estimate the properties of the central cores as well as the analytical model developed and tested by Portegies Zwart & McMillan (2002) for runaway collisions, extended to consider and include mass loss through winds (Fujii et al. 2024; Pacucci et al. 2025), using the wind mass loss rates from Vink (2018). We compared the results of this framework to the direct N-body simulations with stellar evolution from Vergara et al. (2026) for the purpose of verification, finding generally good agreement within a factor of a few, the uncertainty expected within a simplified framework.

We find from the Fokker-Planck model that the formation of cluster cores with masses in the range from $10^4\,{\rm M}_\odot$ up to $10^6\,{\rm M}_\odot$ is expected, with core radii in the range from ∼0.4 pc up to ∼15 pc. Applying the model for the runaway collisions to the different cluster cores, we generally find typical IMBH masses in the range 10^2–$4\times10^3\,{\rm M}_\odot$, where the main parameters that regulate the mass of the IMBH are the mass in the core as well as the metallicity, which regulates the mass loss through winds.

For comparison with the results by Vergara et al. (2024, 2025), we calculated the efficiency to form a massive object, defined as the mass of the massive object divided by the total mass of the cluster. This quantity is plotted as a function of cluster mass divided by critical mass, where the critical mass is the mass for which the collision time of the system is equal to the evolution time of the system (Vergara et al. 2023, 2024). We compared the results to a fit provided by Vergara et al. (2026) to direct N-body simulations, finding good agreement, as both methods yield expected efficiencies in the few percent range. This is the range that is also reasonable to expect for observed systems, as the lifetime of stellar clusters may be very short if they are strongly collision dominated.

We note as a result of these calculations that we can indeed expect the formation of heavy black hole seeds, with masses $M_{\rm BH}\sim10^2$–$4\times10^3\,{\rm M}_\odot$. While the lower end of this mass range is comparable to the $\sim100\,{\rm M}_\odot$ remnants expected from Population III stars (Abel et al. 2002; Bromm et al. 2002), the upper bound extends significantly higher, allowing the most massive clusters to produce objects firmly in the "heavy seed" regime. Forming such heavy seeds is highly beneficial to form SMBHs at high redshift (Sassano et al. 2021). They can also play a relevant role for gravitational wave emission in the context of IMBH mergers, for example in the context of the Laser Interferometer Space Antenna (LISA)[3] and the *Einstein* Telescope[4].

4.1. Implications for little red dots

The LRDs discovered by JWST (Matthee et al. 2024; Greene et al. 2024) exhibit V-shaped spectra often interpreted as broad-line regions powered by SMBHs. Our results suggest that dense massive star clusters could provide possible massive seeds from which the SMBHs in the LRDs may have grown. Particularly, seeds reaching up to $3.7\times10^3\,{\rm M}_\odot$ (as seen in the most massive cluster) formed at $z\sim10$ require significantly fewer e-folding times to reach 10^7–$10^8\,{\rm M}_\odot$ by $z\sim6$ compared to light seeds, alleviating the timing constraints on early SMBH growth (Shapiro 2005). While some scenarios even consider LRDs to be pure stellar systems with very high densities (e.g., Guia et al. 2024), it can be shown that in such systems, collisions could be expected to be very efficient, leading to the formation of very massive central objects in a similar manner as for the dense massive clusters discussed here, but for a higher mass system (Escala et al. 2025; Pacucci et al. 2025). It appears even likely that the LRDs would be in the regime of higher ratios in terms of the mass divided by critical mass, leading potentially to enhanced black hole formation efficiencies in the relation from Vergara et al. (2026).

4.2. Caveats

The model adopted here is a simplified model that is strongly motivated by our current knowledge on runaway collision processes in stellar systems (e.g., Portegies Zwart & McMillan 2002) and has been tested and compared to the direct N-body simulations by Vergara et al. (2026). Nonetheless, the parameters of many of the clusters here are outside of the parameter space that is accessible for direct N-body simulations. We also acknowledge that many of the properties of the clusters are not yet known, including the binary fraction, the rotation in the system, and the internal structure. The initial mass function is also not known; it is possible that it is top-heavy (Jeřábková et al. 2018; Kroupa et al. 2026). This possibility, along with a possible primordial mass segregation, would favor the formation of massive IMBHs, though we did not explore it here in detail.

Other important uncertainties to be considered concern the mass loss in the context of stellar collisions. Numerical simulations initially suggested that mass loss to be on the percent level (e.g., Glebbeek & Pols 2008; Glebbeek et al. 2009), implying only moderate effects in the context of runaway collisions (Alister Seguel et al. 2020). 1D models of stellar pulsation on the other hand suggest that mass loss could also be enhanced, and potentially dominate over the mass gain via collisions (Ramírez-Galeano et al. 2025; Roman-Garza et al. 2026). Particularly, the work of Ramírez-Galeano et al. (2025) shows that the mass loss during collisions depends strongly on the stellar structure and is quite sensitive to the adopted framework for mixing length theory in their calculations, making it crucial to

[3] LISA web page: https://www.esa.int/Science_Exploration/Space_Science/LISA
[4] *Einstein* Telescope web page: https://www.einstein-telescope.it/en/home-en/

arrive at a better understanding on how to model convection in stars for realistic calculations. Roman-Garza et al. (2026) point toward similarly relevant uncertainties, and it will be important to understand through future work if the total unbound mass during a collision will be ejected, or if instead their pulsation-based estimate is more accurate. The current range of models within the literature shows a wide range of uncertainties, from minor effects up to potentially strong limitations for VMS formation (Solar et al. 2025). It will be important for future studies to address this relevant question, including an investigation of pulsations in a 3D framework given the 3D nature of the expected mass loss effects.

Acknowledgements. We thank the anonymous referee for a careful revision of our paper. The authors thank for valuable discussions with Marcelo Vergara, Francesco Flammini Dotti, Abbas Askar, Mirek Giersz, Roberto Capuzzo-Dolcetta, Raffaella Schneider, Lorenzo Paparella, Nathan Leigh and Efrain Vira. DRGS gratefully acknowledges support from the Alexander von Humboldt – Foundation, Bonn, Germany. ML acknowledges financial support from ANID/DOCTORADO BECAS CHILE 72240058. DRGS thanks for funding via the ANID BASAL project FB21003.

References

Abel, T., Bryan, G. L., & Norman, M. L. 2002, Science, 295, 93
Adamo, A., Bradley, L. D., Vanzella, E., et al. 2024, Nature, 632, 513
Akins, H. B., Casey, C. M., Lambrides, E., et al. 2025, ApJ, 991, 37
Alister Seguel, P. J., Schleicher, D. R. G., Boekholt, T. C. N., Fellhauer, M., & Klessen, R. S. 2020, MNRAS, 493, 2352
Arca Sedda, M., Kamlah, A. W. H., Spurzem, R., et al. 2023, MNRAS, 526, 429
Askar, A., Davies, M. B., & Church, R. P. 2022, MNRAS, 511, 2631
Begelman, M. C., & Shlosman, I. 2009, ApJ, 702, L5
Binney, J., Tremaine, S., & Freeman, K. 2009, Phys. Today, 62, 56
Boekholt, T. C. N., Schleicher, D. R. G., Fellhauer, M., et al. 2018, MNRAS, 476, 366
Bromm, V., & Loeb, A. 2003, ApJ, 596, 34
Bromm, V., Coppi, P. S., & Larson, R. B. 2002, ApJ, 564, 23
Brown, G., & Gnedin, O. Y. 2021, MNRAS, 508, 5935
Chang, J. S., & Cooper, G. 1970, J. Comput. Phys., 6, 1
Chassonnery, P., & Capuzzo-Dolcetta, R. 2021, MNRAS, 504, 3909
Chworowsky, K., Finkelstein, S. L., Boylan-Kolchin, M., et al. 2024, AJ, 168, 113
Cohn, H. 1980, ApJ, 242, 765
Davies, M. B., Miller, M. C., & Bellovary, J. M. 2011, ApJ, 740, L42
Dekel, A., Dutta Chowdhury, D., Lapiner, S., et al. 2025, ApJ, submitted [arXiv:2511.07578]
Devecchi, B., & Volonteri, M. 2009, ApJ, 694, 302
Devecchi, B., Volonteri, M., Rossi, E. M., Colpi, M., & Portegies Zwart, S. 2012, MNRAS, 421, 1465
Escala, A. 2021, ApJ, 908, 57
Escala, A., Zimmermann, L., Valdebenito, S., et al. 2025, ApJ, 995, 44
Fujii, M. S., Wang, L., Tanikawa, A., Hirai, Y., & Saitoh, T. R. 2024, Science, 384, 1488
Gaete, B., Schleicher, D. R. G., Lupi, A., et al. 2024, A&A, 690, A378
Glebbeek, E., & Pols, O. R. 2008, A&A, 488, 1017
Glebbeek, E., Gaburov, E., de Mink, S. E., Pols, O. R., & Portegies Zwart, S. F. 2009, A&A, 497, 255
Glebbeek, E., Gaburov, E., Portegies Zwart, S., & Pols, O. R. 2013, MNRAS, 434, 3497
Greene, J. E., Labbe, I., Goulding, A. D., et al. 2024, ApJ, 964, 39
Grudić, M. Y., Hafen, Z., Rodriguez, C. L., et al. 2023, MNRAS, 519, 1366
Guia, C. A., Pacucci, F., & Kocevski, D. D. 2024, Res. Notes Am. Astron. Soc., 8, 207
Gürkan, M. A., Freitag, M., & Rasio, F. A. 2004, ApJ, 604, 632
Inayoshi, K., & Haiman, Z. 2014, MNRAS, 445, 1549
Jeřábková, T., Zonoozi, A. H., Kroupa, P., et al. 2018, A&A, 620, A39
Katz, H., Sijacki, D., & Haehnelt, M. G. 2015, MNRAS, 451, 2352
Koushiappas, S. M., Bullock, J. S., & Dekel, A. 2004, MNRAS, 354, 292
Kroupa, P., Subr, L., Jerabkova, T., & Wang, L. 2020, MNRAS, 498, 5652
Kroupa, P., Gjergo, E., Jerabkova, T., & Yan, Z. 2026, Encyclopedia of Astrophysics, 2, 173
Labbé, I., van Dokkum, P., Nelson, E., et al. 2023, Nature, 616, 266
Latif, M. A., & Schleicher, D. R. G. 2015, A&A, 578, A118
Latif, M. A., Schleicher, D. R. G., Schmidt, W., & Niemeyer, J. 2013, MNRAS, 433, 1607
Latif, M. A., Bovino, S., Grassi, T., Schleicher, D. R. G., & Spaans, M. 2015, MNRAS, 446, 3163
Latif, M. A., Omukai, K., Habouzit, M., Schleicher, D. R. G., & Volonteri, M. 2016, ApJ, 823, 40
Liempi, M., Schleicher, D. R. G., Benson, A., Escala, A., & Vergara, M. C. 2025, A&A, 694, A42
Lupi, A., Colpi, M., Devecchi, B., Galanti, G., & Volonteri, M. 2014, MNRAS, 442, 3616
Marks, M., & Kroupa, P. 2012, A&A, 543, A8
Matthee, J., Naidu, R. P., Brammer, G., et al. 2024, ApJ, 963, 129
Messa, M., Vanzella, E., Loiacono, F., et al. 2026, A&A, 705, A173
Mowla, L. 2024, Nature, 632, 505
Pacucci, F., Hernquist, L., & Fujii, M. 2025, ApJ, 994, 40
Plummer, H. C. 1911, MNRAS, 71, 460
Portegies Zwart, S. F., & McMillan, S. L. W. 2002, ApJ, 576, 899
Ramírez-Galeano, L., Charbonnel, C., Fragos, T., et al. 2025, A&A, 699, A223
Rantala, A., & Naab, T. 2025, MNRAS, 542, L78
Rantala, A., Lahén, N., Naab, T., Escobar, G. J., & Iorio, G. 2025, MNRAS, 543, 2130
Rantala, A., Naab, T., Lahén, N., et al. 2026, MNRAS, 549, stag986
Reinoso, B., Schleicher, D. R. G., Fellhauer, M., Klessen, R. S., & Boekholt, T. C. N. 2018, A&A, 614, A14
Reinoso, B., Schleicher, D. R. G., Fellhauer, M., Leigh, N. W. C., & Klessen, R. S. 2020, A&A, 639, A92
Roman-Garza, J., Fragos, T., Charbonnel, C., et al. 2026, A&A, 707, A163
Sakurai, Y., Yoshida, N., Fujii, M. S., & Hirano, S. 2017, MNRAS, 472, 1677
Sassano, F., Schneider, R., Valiante, R., et al. 2021, MNRAS, 506, 613
Schleicher, D. R. G., Spaans, M., & Glover, S. C. O. 2010, ApJ, 712, L69
Schleicher, D. R. G., Reinoso, B., Latif, M., et al. 2022, MNRAS, 512, 6192
Schleicher, D. R. G., Reinoso, B., & Klessen, R. S. 2023, MNRAS, 521, 3972
Shapiro, S. L. 2005, ApJ, 620, 59
Solar, P. A., Reinoso, B., Schleicher, D. R. G., Klessen, R. S., & Banerjee, R. 2025, A&A, 699, A64
Somerville, R. S., Yung, L. Y. A., Lancaster, L., et al. 2025, MNRAS, 544, 3774
Spitzer, L. 1987, Dynamical Evolution of Globular Clusters
Suazo, M., Prieto, J., Escala, A., & Schleicher, D. R. G. 2019, ApJ, 885, 127
Tagawa, H., Haiman, Z., & Kocsis, B. 2020, ApJ, 892, 36
Vanzella, E., Castellano, M., Bergamini, P., et al. 2022a, A&A, 659, A2
Vanzella, E., Castellano, M., Bergamini, P., et al. 2022b, ApJ, 940, L53
Vanzella, E., Claeyssens, A., Welch, B., et al. 2023, ApJ, 945, 53
Vanzella, E., Messa, M., Adamo, A., et al. 2026, A&A, 705, A171
Vasiliev, E. 2017, ApJ, 848, 10
Vasiliev, E. 2019, MNRAS, 482, 1525
Vergara, M. Z. C., Schleicher, D. R. G., Boekholt, T. C. N., et al. 2021, A&A, 649, A160
Vergara, M. C., Escala, A., Schleicher, D. R. G., & Reinoso, B. 2023, MNRAS, 522, 4224
Vergara, M. C., Schleicher, D. R. G., Escala, A., et al. 2024, A&A, 689, A34
Vergara, M. C., Askar, A., Kamlah, A. W. H., et al. 2025, A&A, 704, A321
Vergara, M. C., Askar, A., Flammini Dotti, F., et al. 2026, A&A, 707, A71
Vink, J. S. 2018, A&A, 615, A119
Wise, J. H., Turk, M. J., & Abel, T. 2008, ApJ, 682, 745
Yoshida, N., Omukai, K., & Hernquist, L. 2008, Science, 321, 669
Zhang, Y., Ding, X., Yang, L., et al. 2025, arXiv e-prints [arXiv:2510.25830]